Three major categories of nanotube structures can be identified based on the values of *m* and *n*

***m* = *n* "Armchair"**
***m* = 0 or *n* = 0 "Zigzag"**
***m* ≠ *n* "Chiral"**

Nature 391, 59, (1998)

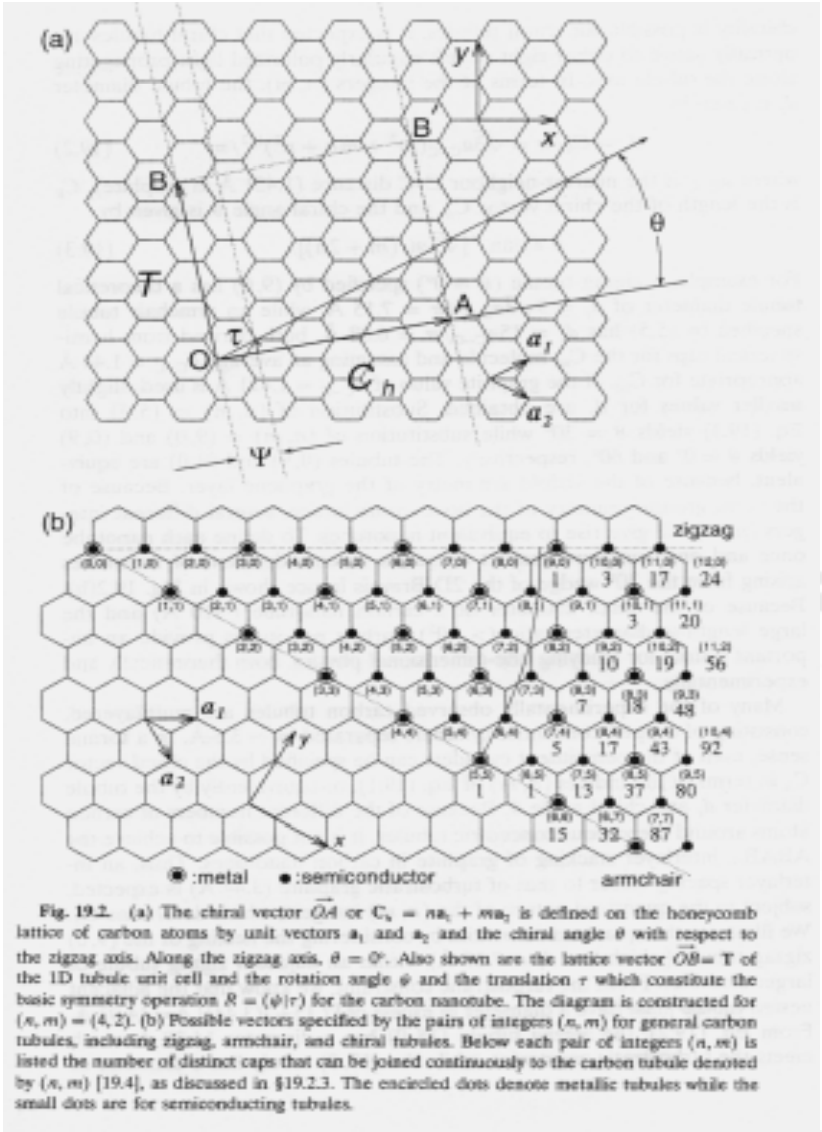

Fig. 19.2. (a) The chiral vector $\vec{OA}$ or $\mathbf{C}_h = n\mathbf{a}_1 + m\mathbf{a}_2$ is defined on the honeycomb lattice of carbon atoms by unit vectors $\mathbf{a}_1$ and $\mathbf{a}_2$ and the chiral angle θ with respect to the zigzag axis. Along the zigzag axis, $\theta = 0°$. Also shown are the lattice vector $\vec{OB} = \mathbf{T}$ of the 1D tubule unit cell and the rotation angle ϕ and the translation τ which constitute the basic symmetry operation $R = (\phi|\tau)$ for the carbon nanotube. The diagram is constructed for $(n, m) = (4, 2)$. (b) Possible vectors specified by the pairs of integers (n, m) for general carbon tubules, including zigzag, armchair, and chiral tubules. Below each pair of integers (n, m) is listed the number of distinct caps that can be joined continuously to the carbon tubule denoted by (n, m) [19.4], as discussed in §19.2.3. The encircled dots denote metallic tubules while the small dots are for semiconducting tubules.

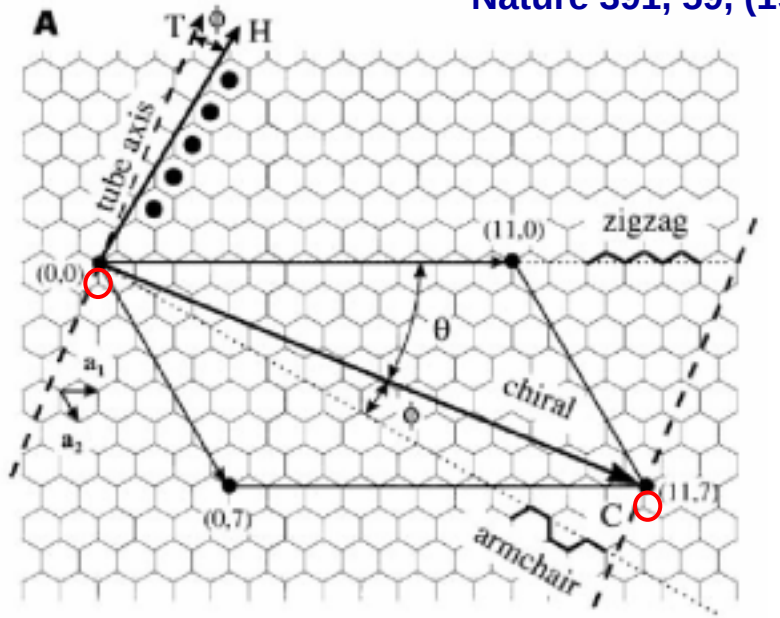

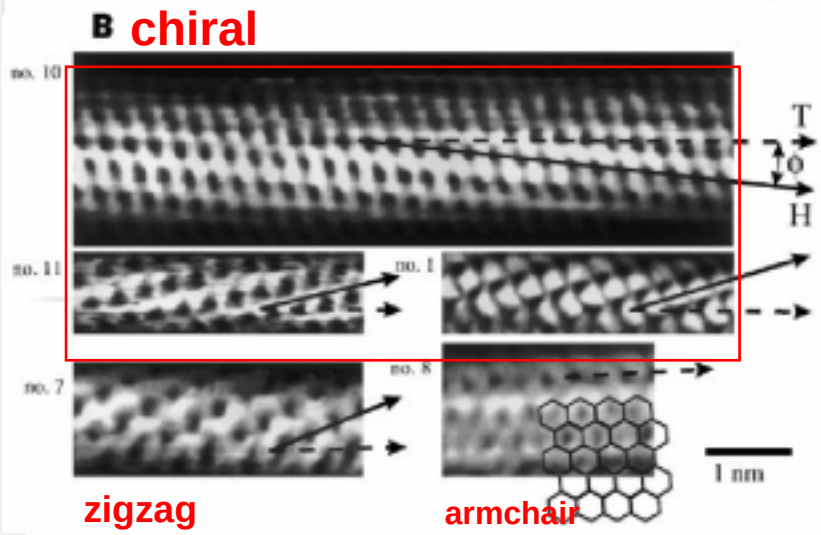

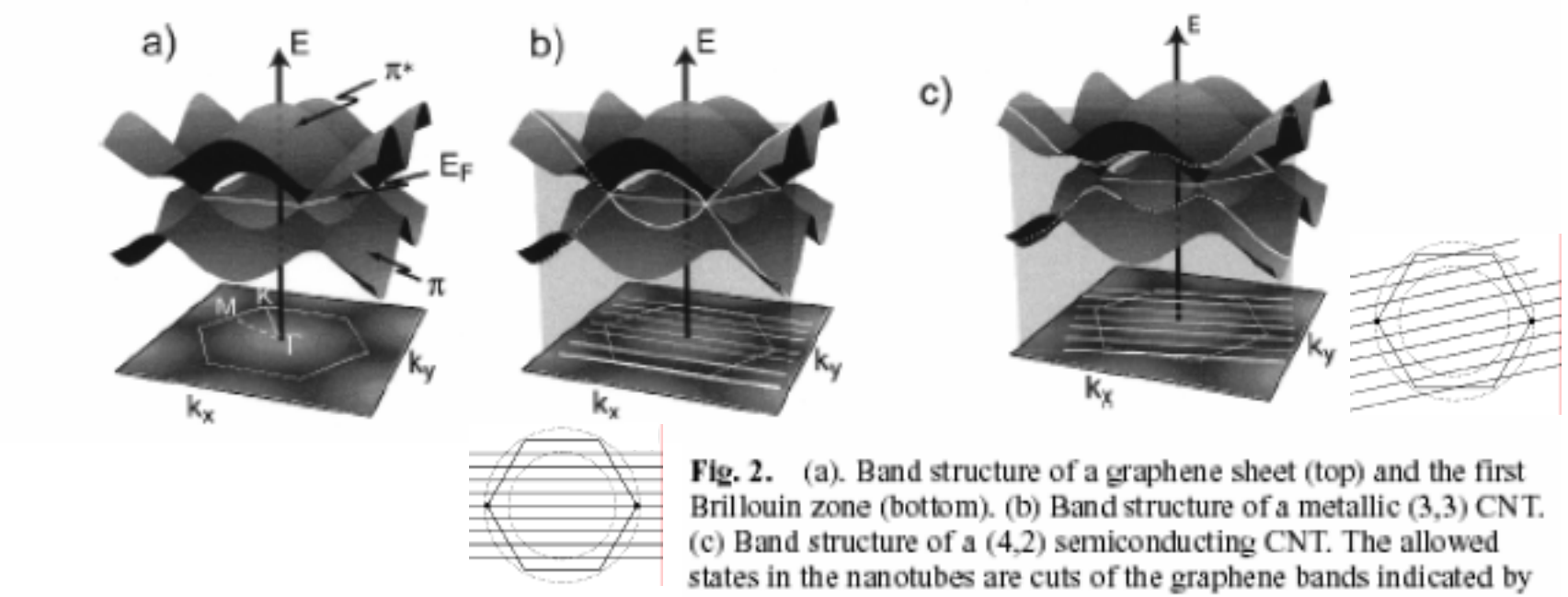

Fig. 2. (a). Band structure of a graphene sheet (top) and the first Brillouin zone (bottom). (b) Band structure of a metallic (3,3) CNT. (c) Band structure of a (4,2) semiconducting CNT. The allowed states in the nanotubes are cuts of the graphene bands indicated by the white lines. If the cut passes through a K point, the CNT is metallic; otherwise, the CNT is semiconducting.

J. Tersoff, APL, 74, 2122, (99)
http://www.ece.eng.wayne.edu/~jchoi/06012004.pdf

a) Graphite

Valence(π) and Conduction (π^*) states touch at 6 Fermi points

Carbon nanotube:

Quantization from the confinement of electrons in the circumferential direction

circumference = $n\lambda_F$

b) (3,3) CNT; allowed energy states of CNT cuts pass through Fermi point → metallic

c) (4,2) CNT; no cut pass through a K point ⟶ semiconducting

$$E_{gap} = \frac{4\hbar v_F}{3d_{CNT}}$$

In general, for a chiral tubule, we have the following results:

n - m = 3q metallic, no gap

n - m ≠ 3q semiconductor with gap

$$d_{CNT} = \frac{2.46\sqrt{n^2 + nm + m^2}}{2\pi}\ \text{nm}$$

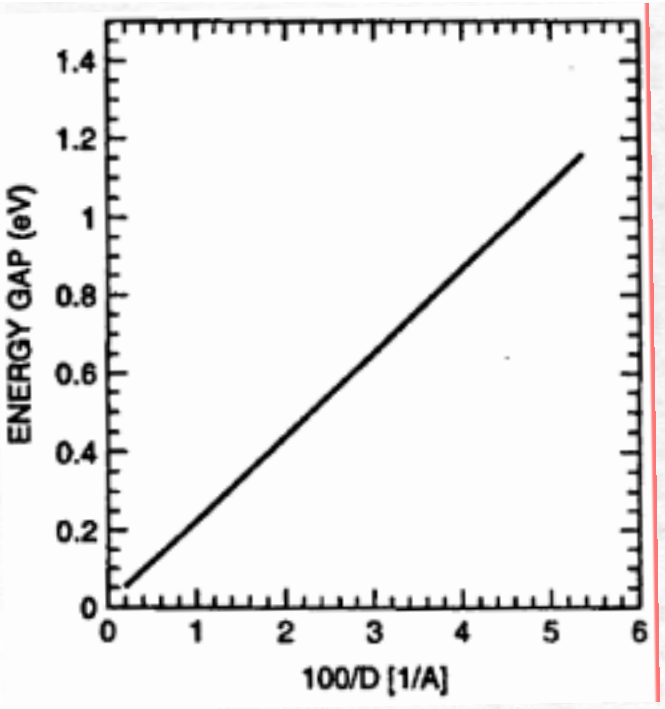

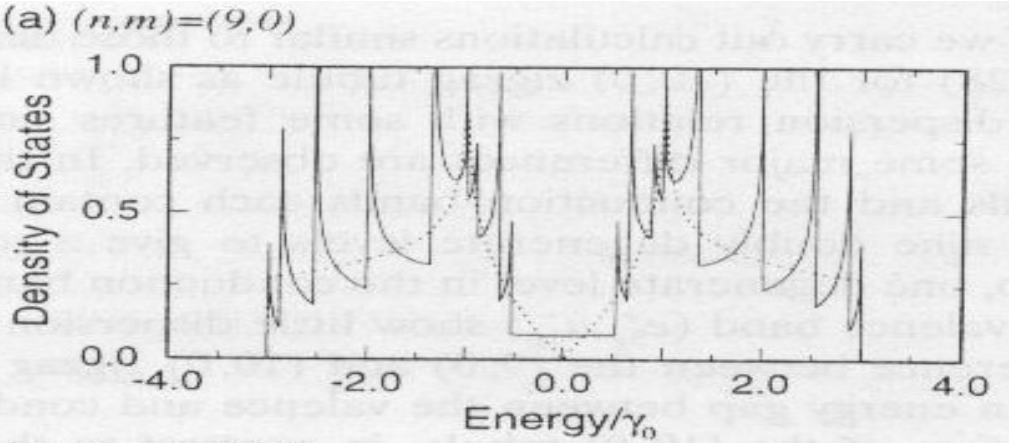

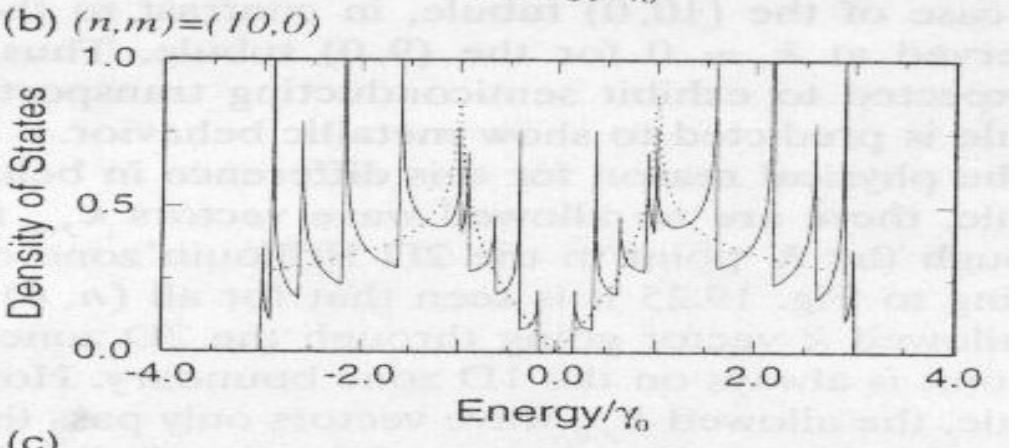

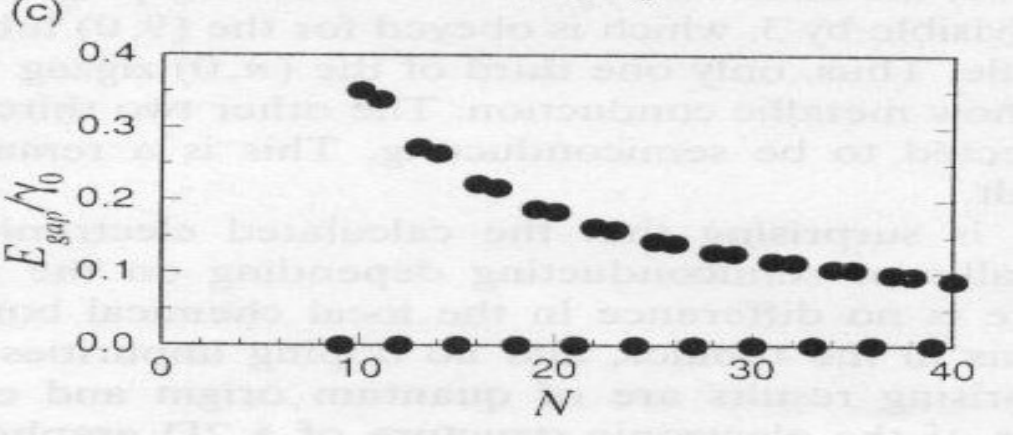

Fig. 19.27. Electronic 1D density of states per unit cell for two (n, m) zigzag tubules based on zone folding of a 2D graphene sheet: (a) the (9, 0) tubule which has metallic behavior, (b) the (10, 0) tubule which has semiconducting behavior. Also shown in the figure is the density of states for the 2D graphene sheet (dashed curves) [19.98]. (c) Plot of the energy gap for $(n, 0)$ zigzag nanotubes plotted in units of γ_0 as a function of n, where γ_0 is the energy of the nearest-neighbor overlap integral for graphite [19.100].

≈2.5eV

Cross-section view of the vibration modes

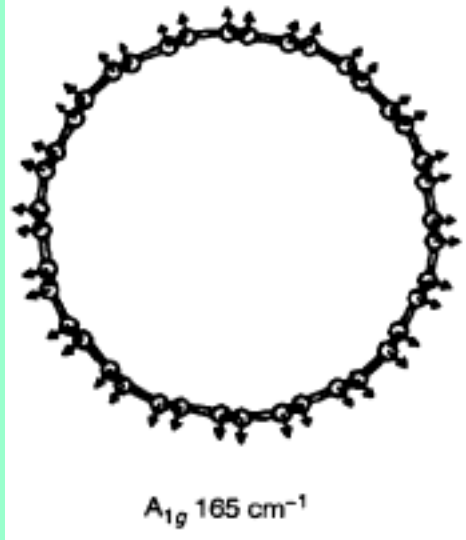

Symmetric stretch

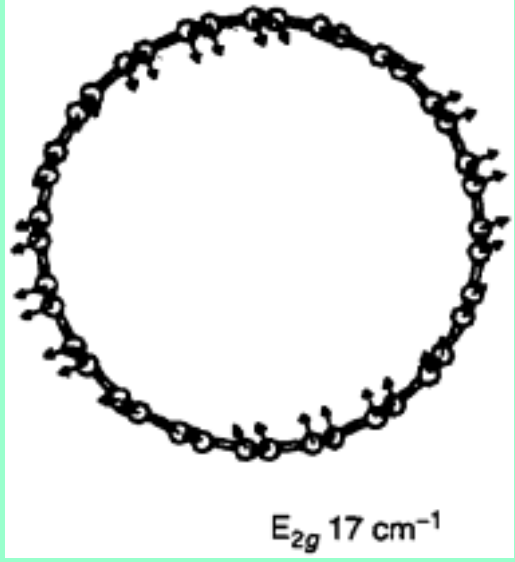

Asymmetric stretch

Determination of the tube diameter from A_{1g} Raman vibration frequency

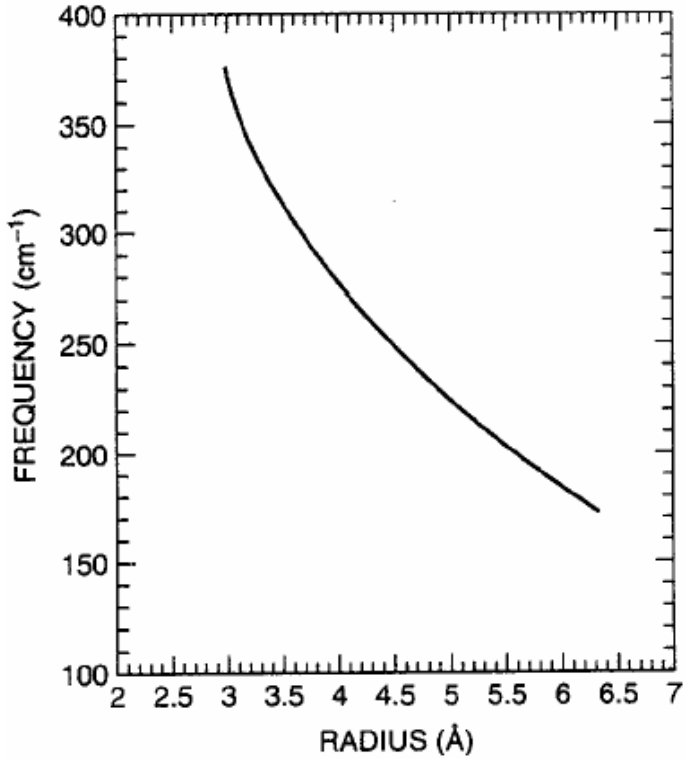

One can then "guess" a set of (m,n) from

$$d_{CNT} = \frac{2.46\sqrt{n^2 + nm + m^2}}{2\pi} \text{ nm}$$

Figs. 5-19 and 5-20

A SWCNT CMOS device

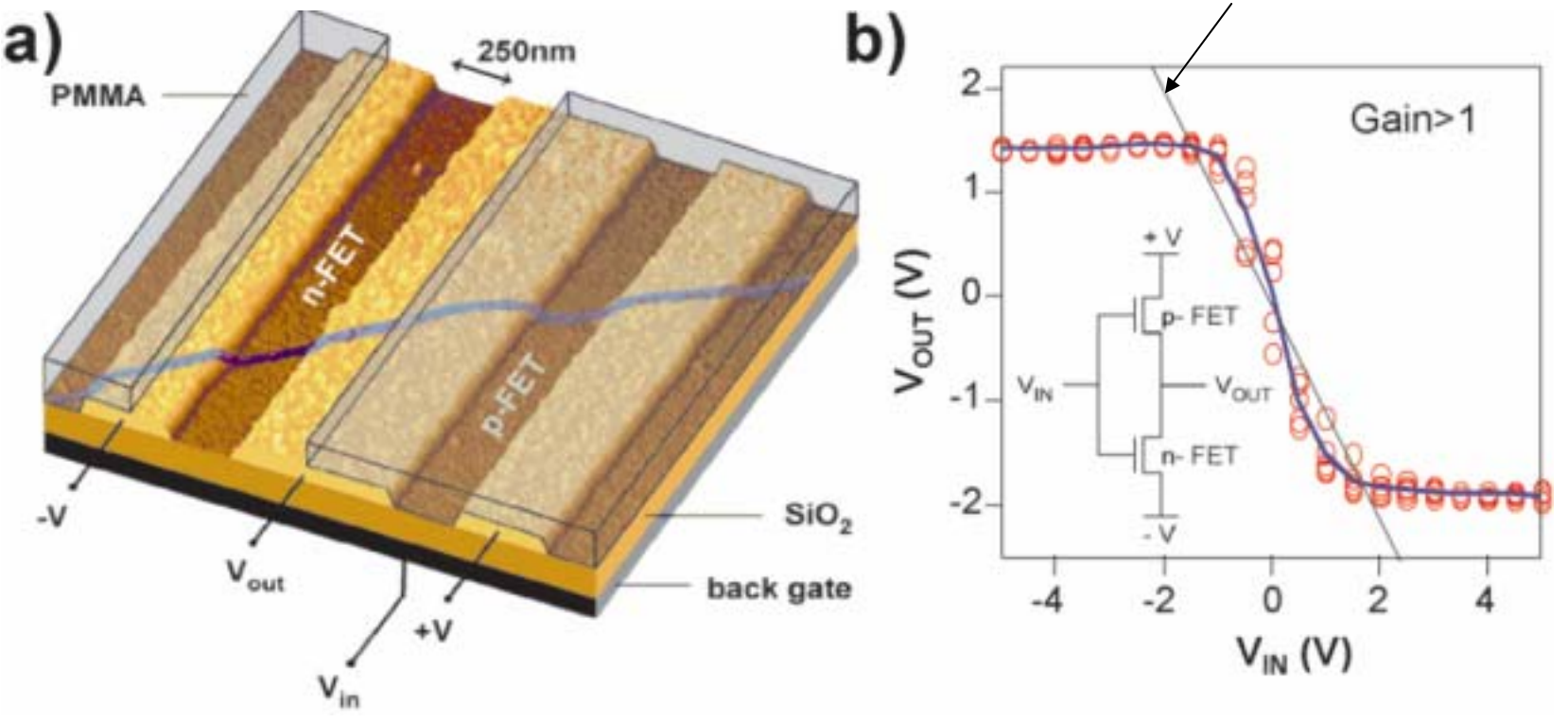

1. Two p-type CNT FETs in series
2. Potassium bombardment on the unprotected one results in a p→n conversion
3. CMOS CNT FET with gain ≡ (V_{out}/V_{in}) > 1

Introduction to Nanotechnology

Chapter 9 Quantum Wells, Wires and Dots
Lecture 2

ChiiDong Chen
Institute of Physics, Academia Sinica
chiidong@phys.sinica.edu.tw
02 27896766

Size effect:

For a nano-meter cube, the surface to volume ratio increases with decreasing size

For an FCC cubic: $N_{surface} = 12\ n^2$

$N_{volume} = 8n^3 + 6n^2 + 3n$

n = number of atoms along edges
d = na, a = lattice constant

For GaAs, a=0.565 nm

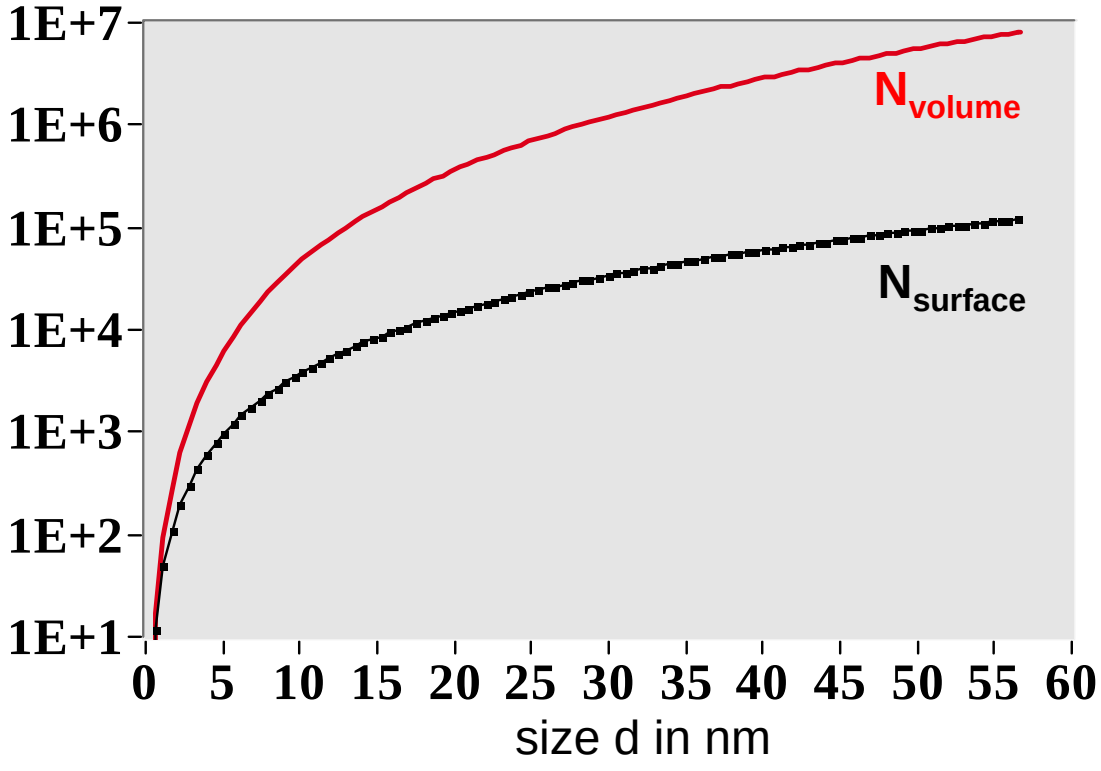

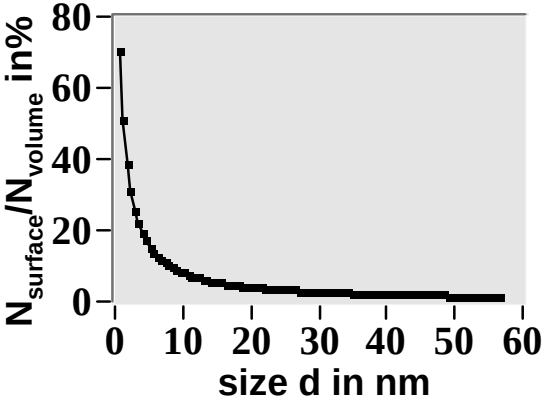

Charge motion in a conductor or semiconductor with periodic crystal potential:

Resistance arises from scattering with phonons and defects

Force on an electron $F=eE$ Momentum $P=mv=F\Delta t$; $\Delta t=\tau$ $\Rightarrow v = \tau eE/m$

τ = average scattering time mean free path $l = v_F \tau$

Ohm's law:

current density $j = nev = \dfrac{ne^2\tau E}{m}$ $j \equiv \sigma E \rightarrow \sigma = \dfrac{ne^2\tau}{m} \rightarrow \rho \equiv \dfrac{1}{\sigma} = \dfrac{m}{ne^2\tau}$

mobility: $\mu \equiv \dfrac{v}{E} = \dfrac{\tau e}{m}$

Scattering time: $\dfrac{1}{\tau} = \dfrac{1}{\tau_L} + \dfrac{1}{\tau_i}$

For $T>>\Theta_D$: $\rho \sim T$

For $T<<\Theta_D$: $\rho \sim T^3$

For $T<<<\Theta_D$: $\rho \sim T^5$

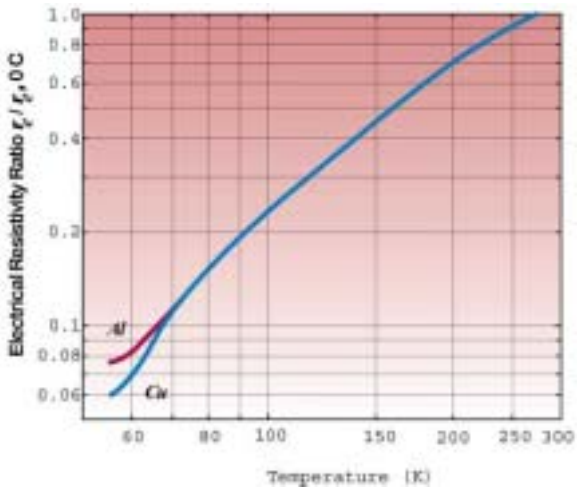

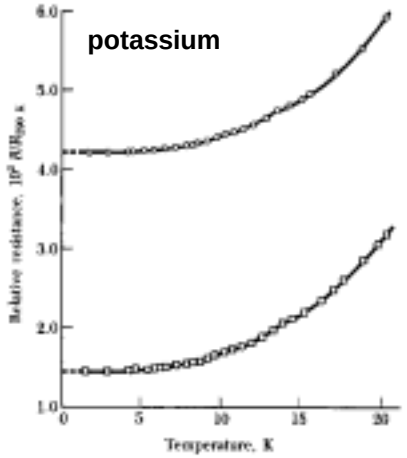

Barron, R. F., Cryogenic Systems, 2nd Edition, Oxford University Press, New York, 1985

http://www.electronics-cooling.com/html/2001_august_a3.html

Residual resistivity: 1% atomic impurity = 1μΩ-cm

Types of defects:

1. mission atoms ≡ vacancies
2. extra atoms ≡ interstitial atoms
3. a vacancy – interstitial atom pair ≡ Frenkel defect

in semiconductors:

doping level of 10^{14}~10^{18} donors/cm^3

→ 10^{-1}~10^{3} conduction electrons in (100nm)^3 cube

10 cubes share one electron

Table 9.2. Conduction electron content of smaller size (on left) and larger size (on right) quantum structures containing donor concentrations of 10^{14}–10^{18} cm^{-3}

Quantum Structure	Size	Electron Content	Size	Electron Content
Bulk material	—	10^{14}–10^{18} cm^{-3}	—	10^{14}–10^{18}cm^{-3}
Quantum well	10 nm thick	1–10^{4} μm^{-2}	100 nm thick	10–10^{5} μm^{-2}
Quantum wire	10 × 10-nm cross section	10^{-2}–10^{2} μm^{-1}	100 nm × 100 nm cross section	1–10^{4} μm^{-1}
Quantum dot	10 nm on a side	10^{-4}–1	100 nm on a side	10^{-1}–10^{3}

Sec. 9.3.2 Dimensionality

Example: a 2D Cu film: 10cm×10cm×3.6nm

20% of atoms are in unit cells at the surface → confinement of electron in vertical direction

Length scales for electron motion: mean free path; Fermi wavelength

Relevant scale: Fermi wavelength

Sec. 9.3.3 Fermi Gas and Density of States

Classical description: Momentum $p = mv$ Kinetic Energy $E = mv^2/2 = p^2/2m$

Quantum description: $p_x = \hbar k_x$

All conduction electrons are equally spread out in the k space (reciprocal space)

Available space in k

Table A.1. Properties of coordinate and k space in one, two, and three dimensions

Coordinate Region	k-Space Unit Cell	Fermi Region	Value of k^2	Dimensions
Length L	$2\pi/L$	$2k_F$	k_x^2	One
Area $A = L^2$	$(2\pi/L)^2$	πk_F^2	$k_x^2 + k_y^2$	Two
Volume $V = L^3$	$(2\pi/L)^3$	$4\pi k_F^3/3$	$k_x^2 + k_y^2 + k_z^2$	Three

Table A.2. Number of electrons $N(E)$ and density of states $D(E) = dN(E)/dE$ as function of energy E for electrons delocalized in one, two, and three spatial dimensions, where $A = L^2$ and $V = L^3$

Number of Electrons N	Density of States $D(E)$	Delocalization Dimensions
$N(E) = \frac{4k_F \cdot}{2\pi/L} = \frac{2L}{\pi}\left(\frac{2m}{\hbar^2}\right)^{1/2} E^{1/2}$	$D(E) = \frac{L}{\pi}\left(\frac{2m}{\hbar^2}\right)^{1/2} E^{-1/2}$	1
$N(E) = \frac{2\pi k_F^2 \cdot}{(2\pi/L)^2} = \frac{A}{2\pi}\left(\frac{2m}{\hbar^2}\right) E$	$D(E) = \frac{A}{2\pi}\left(\frac{2m}{\hbar^2}\right)$	2
$N(E) = \frac{2(4\pi k_F^3/3) \cdot}{(2\pi/L)^3} = \frac{V}{3\pi^2}\left(\frac{2m}{\hbar^2}\right)^{3/2} E^{3/2}$	$D(E) = \frac{V}{2\pi^2}\left(\frac{2m}{\hbar^2}\right)^{3/2} E^{1/2}$	3

$\frac{dN(E)}{dE}$

Confined electron wavefunction in a infinite square well

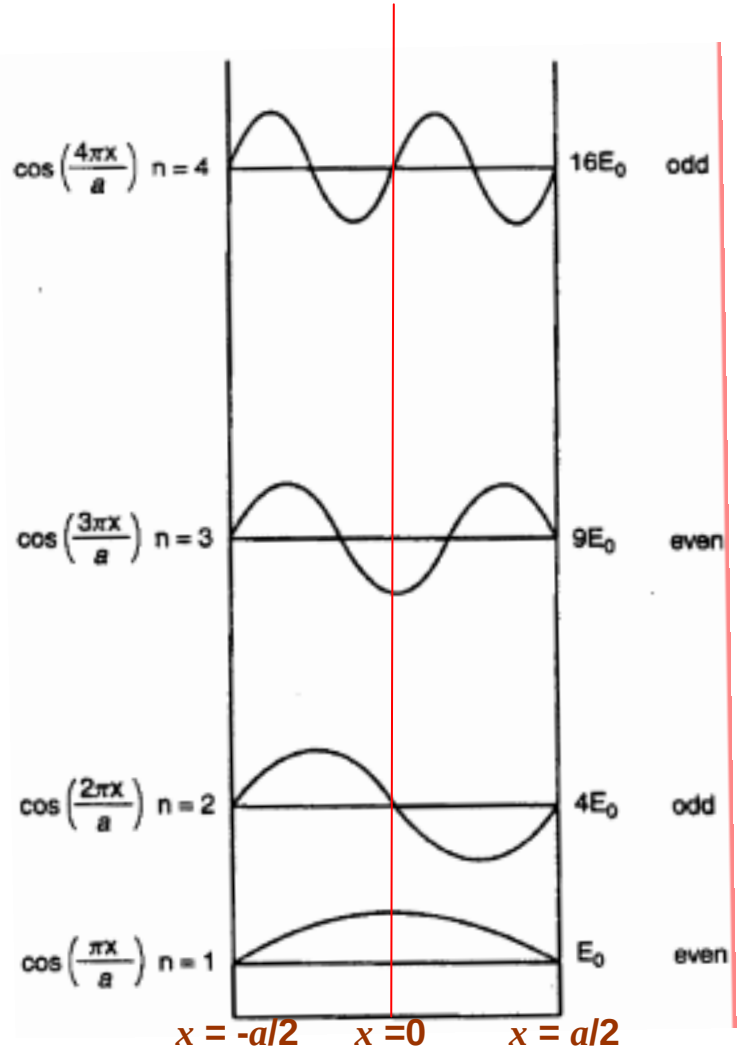

$$n = \frac{2k_F}{2\pi/a} = \frac{a}{\pi}\left(\frac{2m}{\hbar^2}\right)^{1/2} E_n^{1/2}$$

c.f. 1D in Table A2

Let L=*a*, do not need to consider spin

$$E_n = \left[\frac{\pi^2\hbar^2}{2ma^2}\right]n^2$$

$\psi_n = \cos(n\pi x/a)$ $n = 1,3,5,\ldots$ *even parity*

$\psi_n(-x) = \psi_n(x)$

$\psi_n = \sin(n\pi x/a)$ $n = 2,4,6,\ldots$ *odd parity*

$\psi_n(-x) = -\psi_n(x)$

Probability of finding an electron at a particular value of $x = |\Psi_n(x)|^2$

Energy levels for a 1D parabolic potential well

$$V(x) = \frac{1}{2}kx^2 \quad E_n = \left(n - \frac{1}{2}\right)\hbar\omega_0 \quad \omega_0 = \sqrt{\frac{k}{m}}$$

$$\psi_n(x) = H_n(x)\, e^{-\frac{\alpha x^2}{2}}$$

Fig. 9.14

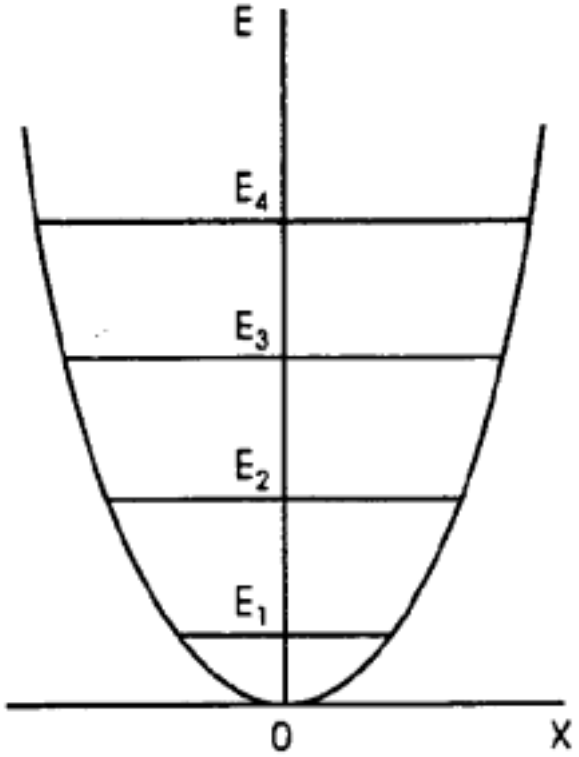

Hermite polynomials $H_n(x)$

n= 0	1
1	$2x$
2	$4x^2 - 2$
3	$8x^3 - 12x$
4	$16x^4 - 48x^2 + 12$
5	$32x^5 - 160x^3 + 120x$
6	$64x^6 - 480x^4 + 720x^2 - 120$
7	$128x^7 - 1344x^5 + 3360x^3 - 1680x$
8	$256x^8 - 3584x^6 + 13440x^4 - 13440x^2 + 1680$
9	$512x^9 - 9216x^7 + 48384x^5 - 80640x^3 + 30240x$
10	$1024x^{10} - 23040x^8 + 161280x^6 - 403200x^4 + 302400x^2 - 30240.$

Degeneracy:

Energy of a 2D infinite rectangular square

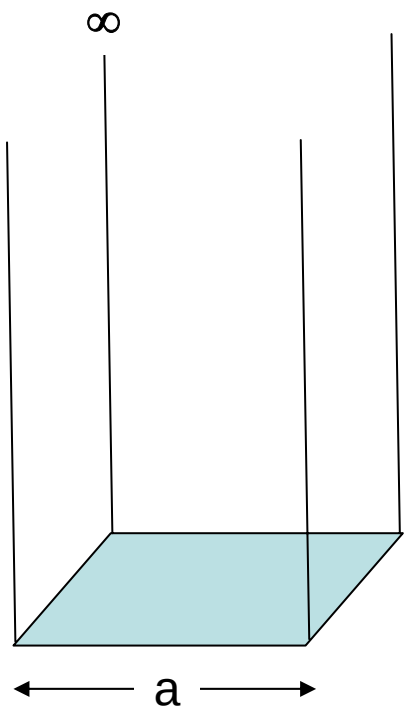

$$E_n = \left(\frac{\pi^2 \hbar^2}{2ma^2} \right) \left(n_x^2 + n_y^2 \right) = E_0 n^2$$ eq. 9.9

Degeneracy (including spin states) :

n	degeneracy	n_x, n_y	n_x, n_y	n_x, n_y	n_x, n_y
1	**4**	**0,1**	**1,0**		
2	**4**	**0,2**	**2,0**		
3	**4**	**0,3**	**3,0**		
4	**4**	**0,4**	**4,0**		
5	**8**	**0,5**	**5,0**	**2,3**	**3,2**

N(E) and D(E) in 1D, 2D and 3D

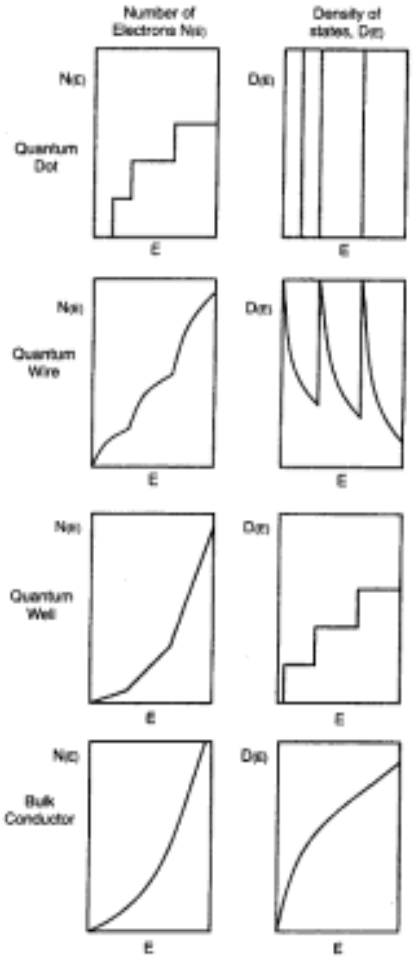

Table A.2. Number of electrons $N(E)$ and density of states $D(E) = dN(E)/dE$ as function of energy E for electrons delocalized in one, two, and three spatial dimensions, where $A = L^2$ and $V = L^3$

Number of Electrons N	Density of States $D(E)$	Delocalization Dimensions
$N(E) = \frac{4k_F}{2\pi/L} = \frac{2L}{\pi}\left(\frac{2m}{\hbar^2}\right)^{1/2} E^{1/2}$	$D(E) = \frac{L}{\pi}\left(\frac{2m}{\hbar^2}\right)^{1/2} E^{-1/2}$	1
$N(E) = \frac{2\pi k_F^2}{(2\pi/L)^2} = \frac{A}{2\pi}\left(\frac{2m}{\hbar^2}\right) E$	$D(E) = \frac{A}{2\pi}\left(\frac{2m}{\hbar^2}\right)$	2
$N(E) = \frac{2(4\pi k_F^3/3)}{(2\pi/L)^3} = \frac{V}{3\pi^2}\left(\frac{2m}{\hbar^2}\right)^{3/2} E^{3/2}$	$D(E) = \frac{V}{2\pi^2}\left(\frac{2m}{\hbar^2}\right)^{3/2} E^{1/2}$	3

Table A.3. Number of electrons $N(E)$ and density of states $D(E) = dN(E)/dE$ as a function of the energy E for electrons delocalized/confined in quantum dots, quantum wires, quantum wells, and bulk material[a]

Type	Number of Electrons N	Density of States $D(E)$	Dimensions: Delocalized	Dimensions: Confined
Dot	$N(E) = 2\Sigma d_i \Theta(E - E_{i_{dot}})$	$D(E) = 2\Sigma d_i \delta(E - E_{i_{dot}})$	0	3
Wire	$N(E) = \frac{2L}{\pi}\left(\frac{2m}{\hbar^2}\right)^{1/2} \Sigma d_i (E - E_{i_{wire}})^{1/2}$	$D(E) = \frac{L}{\pi}\left(\frac{2m}{\hbar^2}\right)^{1/2} \Sigma d_i (E - E_{i_{wire}})^{-1/2}$	1	2
Well	$N(E) = \frac{A}{2\pi}\left(\frac{2m}{\hbar^2}\right) \Sigma d_i (E - E_{i_{well}})$	$D(E) = \frac{A}{2\pi}\left(\frac{2m}{\hbar}\right) \Sigma d_i$	2	1
Bulk	$N(E) = \frac{V}{3\pi^2}\left(\frac{2m}{\hbar^2}\right)^{3/2} (E)^{3/2}$	$D(E) = \frac{V}{2\pi^2}\left(\frac{2m}{\hbar^2}\right)^{3/2} (E)^{1/2}$	3	0

[a]The degeneracies of the confined (square or parabolic well) energy levels are given by d_i. The Heaviside step function $\Theta(x)$ is zero for $x < 0$ and one for $x > 0$; the delta function $\delta(x)$ is zero for $x \neq 0$, infinity for $x = 0$, and integrates to a unit area.

Measurement of electronic density of state at the Fermi level: D(EF)

1. heat capacity at low temperature $C_{el} = \pi^2 D(E_F) k_B^2 T/3$

2. Pauli susceptibility $\chi_{el} = \mu_B^2 D(E_F)$

note:
1. $\chi \equiv M/H$
2. no temperature dependence

3. Spectrum of e-beam induced X-ray

Other methods:

Photoemission spectroscopy, Seebeck effect, tunneling effect

Excitons:

Rydberg series

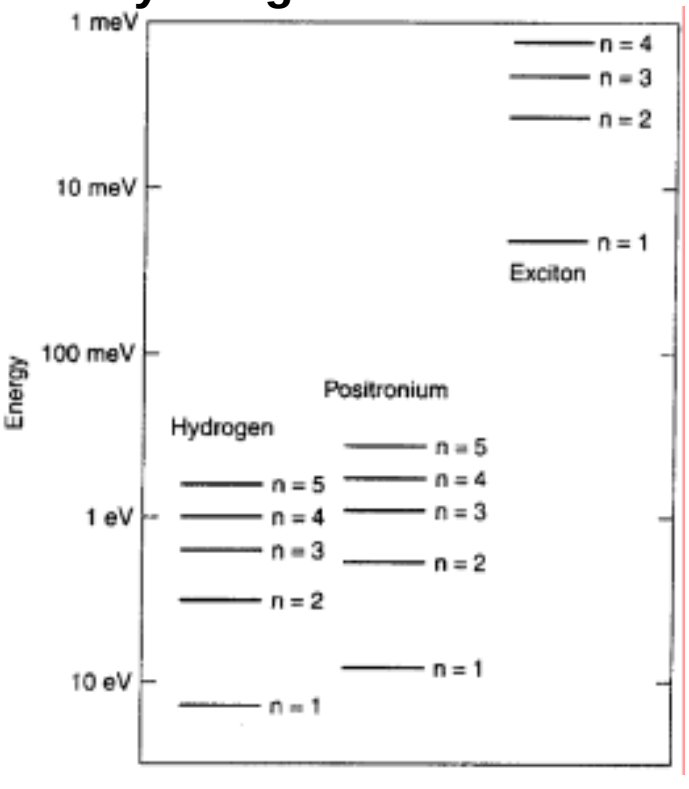

Radius of an exciton:

$$a_{eff} = 0.0529\ (\varepsilon/\varepsilon_0) / (m^*/m_0)\ \text{nm}$$

In semiconductors, large ε,

→ **screening effect**

→ **reduced e-h interation**

→ **a_{eff} >> lattice spacing**

Mott-Wannier exciton

For GaAs: $\varepsilon/\varepsilon_0 = 13.2$, $m^*/m_0 = 0.067$

→ **$a_{eff} = 10.4$ nm**

$d >> a_{eff}$: no confinement

$d > a_{eff}$: weak confinement

$d < a_{eff}$: strong confinement

Increasing e-h interaction

blue shift

in optical absorption

Single Electron Tunneling

Capacitance of a dielectric disk : $C = 8\varepsilon_0\varepsilon_r r$

Capacitance of a dielectric sphere : $C = 4\varepsilon_0\varepsilon_r r$

For a GaAs sphere, $C = 1.47 \times 10^{-18} r$ farad for radius r in nm

VOLUME 63, NUMBER 7 p. 801 PHYSICAL REVIEW LETTERS 14 AUGUST 1989

Scanning-Tunneling-Microscope Observations of Coulomb Blockade and Oxide Polarization in Small Metal Droplets

R. Wilkins,[1] E. Ben-Jacob,[1,2] and R. C. Jaklevic[3]

[1]*Department of Physics, The University of Michigan, Ann Arbor, Michigan 48109*

[2]*School of Physics and Astronomy, Raymond and Beverly Sackler Faculty of Exact Sciences, Tel Aviv University, 69978 Tel Aviv, Israel*

[3]*Scientific Laboratory, Ford Motor Company, Dearborn, Michigan 48121*

(Received 20 March 1989)

C≈7aF for ε_r=10

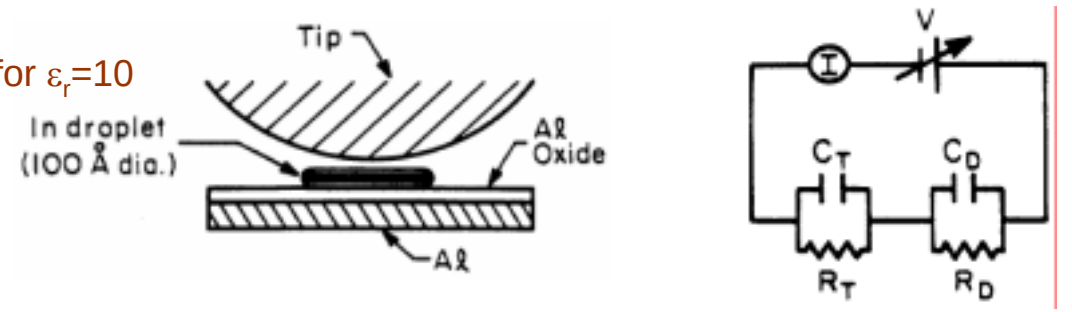

FIG. 1. Schematic showing an In droplet separated from an Al ground plane by a tunneling oxide layer (≃10 Å thickness) with an Au STM tip positioned about 10 Å above it. The equivalent circuit is shown with a voltage source and capacitor C_T for tip to droplet and C_D for droplet to ground plane. The resistors characterize the tunneling probability for each junction and are strictly shot-noise devices.

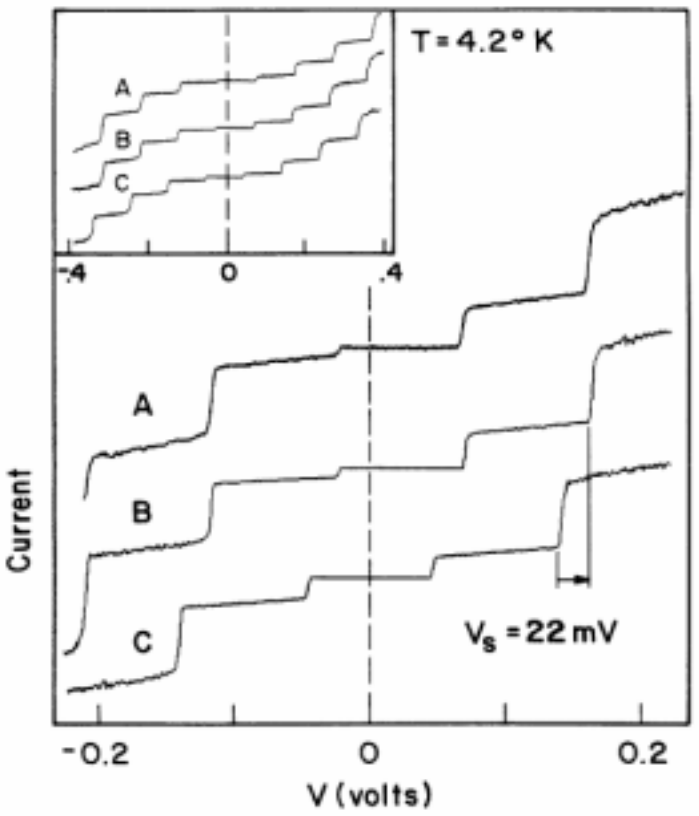

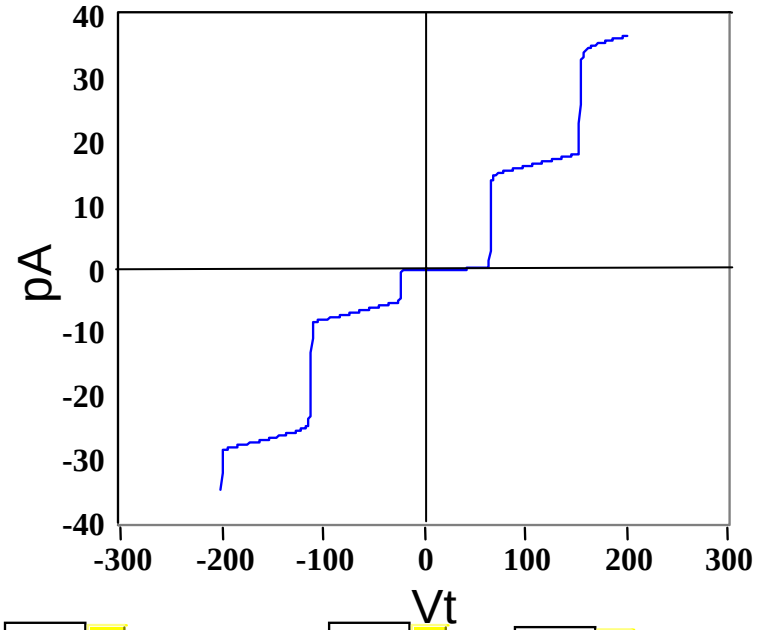

Ct 350.0 zF Cd 1.8 aF Cg 0.01 aF $\frac{Vp}{Vg} = \frac{C_g}{C_t + C_d}$

Rt 4.40 GOhm Rd 7.20 MOhm Vg 3.87 V

$$V_D = \frac{VC_T}{C_D + C_T} + \frac{Ne}{C_D + C_T} + V_p$$

FIG. 2. Curve A is an experimental I-V characteristic from an In droplet in a sample with average droplet size of 300 Å. The peak-peak current is 1.8 nA. Curve B is a theoretical fit to the data for $C_D = 3.5 \times 10^{-19}$ F, $C_T = 1.8 \times 10^{-18}$ F, $R_D = 7.2 \times 10^6$ Ω, and $R_T = 4.4 \times 10^9$ Ω. The obvious asymmetric features in curve A require a voltage shift $V_s = 22$ mV ($V_p = 18$ mV). Curve C, calculated for $V_s = 0$, shows the (seldom observed) symmetric case. As explained in the text, a small quadratic term was added to the computed tunneling rate for each junction. Inset: A wider voltage scan for this same droplet; again, the topmost curve is experimental data.

by scanning the substrate.[14] However, we do not understand at this time why C_T is greater than C_D. At $T = 4$

Asymmetric SET (simulations)

Coulomb Staircase

R_1= 50 kΩ, R_2= 1 MΩ, C_1=0.2fF, C_2=0.15fF, C_g=16aF,
E_C=2.54K, T=20mK

appears when $R_1C_1 \neq R_2C_2$

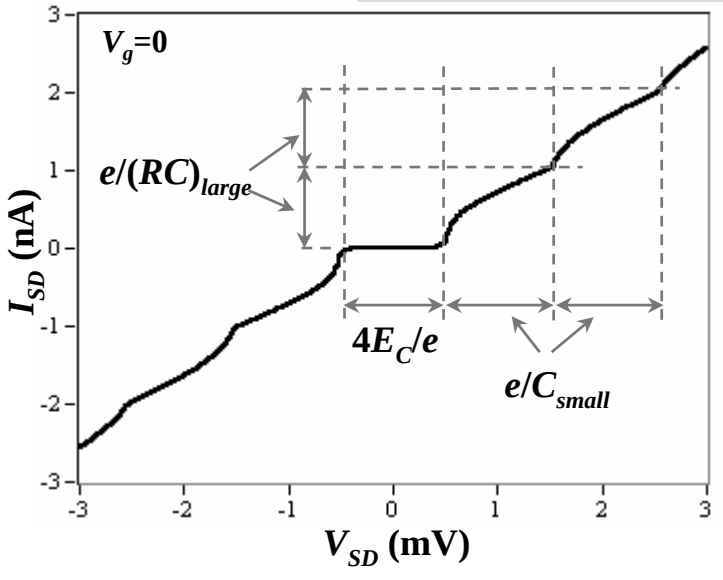

appears when $R_1 \neq R_2$

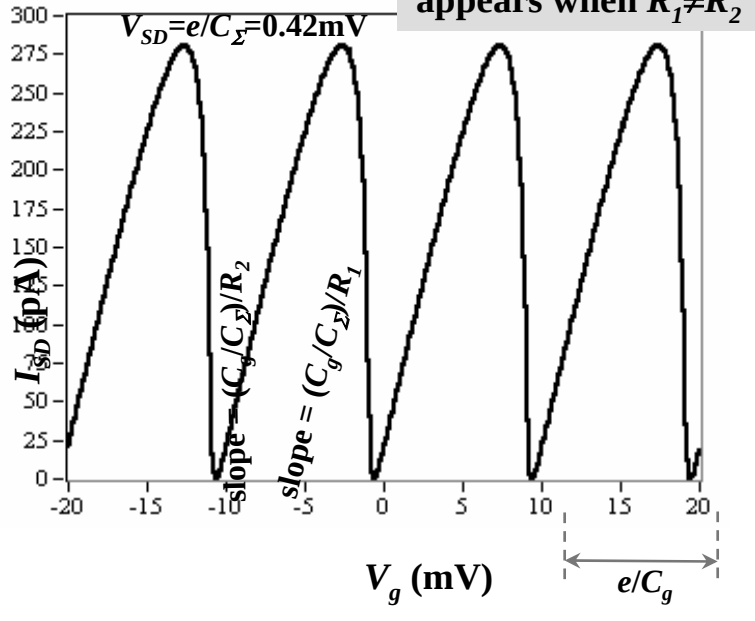

Potential distribution in a finite 1-D array of arbitrary mesoscopic tunnel junctions

V. Gasparian[1], U. Simon*

Institut für Anorganische Chemie, Festkörperchemie, Universität GH Essen, Schützenbahn 70, Essen 45127, Germany

Received 2 September 1997

Physica B 240 (1997) 289–297

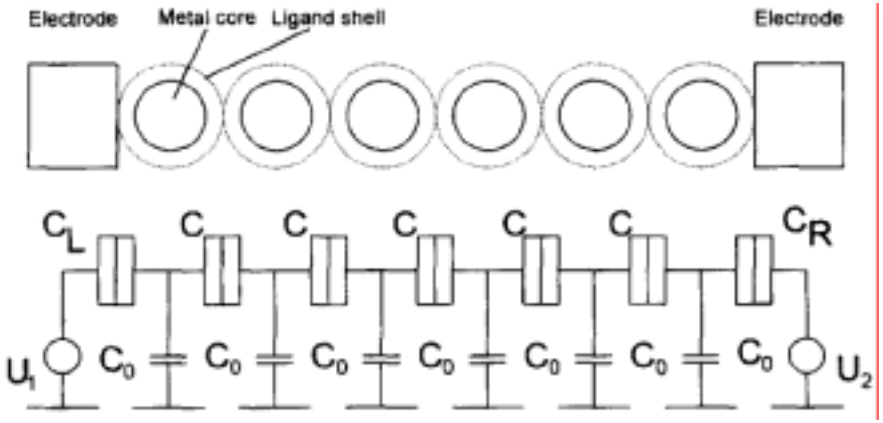

$$-\varphi_i = \frac{e}{C_{eff}}\Pi^{|i-k|}$$

$$\Pi \equiv x - \sqrt{x^2 - 1} \qquad C_{eff} = \sqrt{C_0^2 + 4CC_0}$$

$$x = 1 + C_0/2C$$

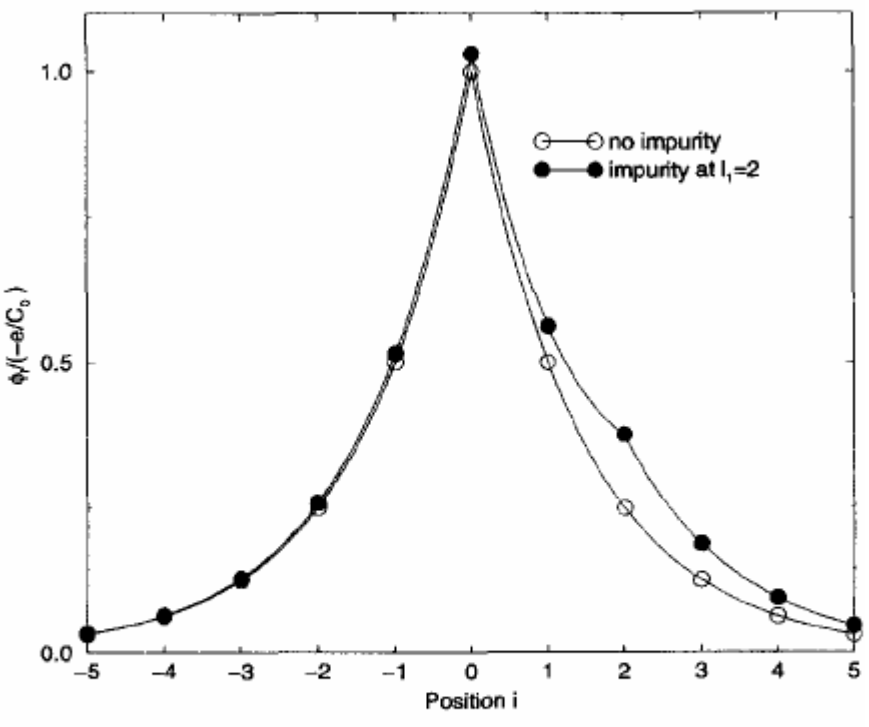

Fig. 2. Potential distribution of the infinite array in the units of $-e/C_0$ and for one impurity at $l_1 = 2$ with $C_1/C_0 = -0.999$.

IV characteristics for 1D array with C=100aF, R=20kΩ

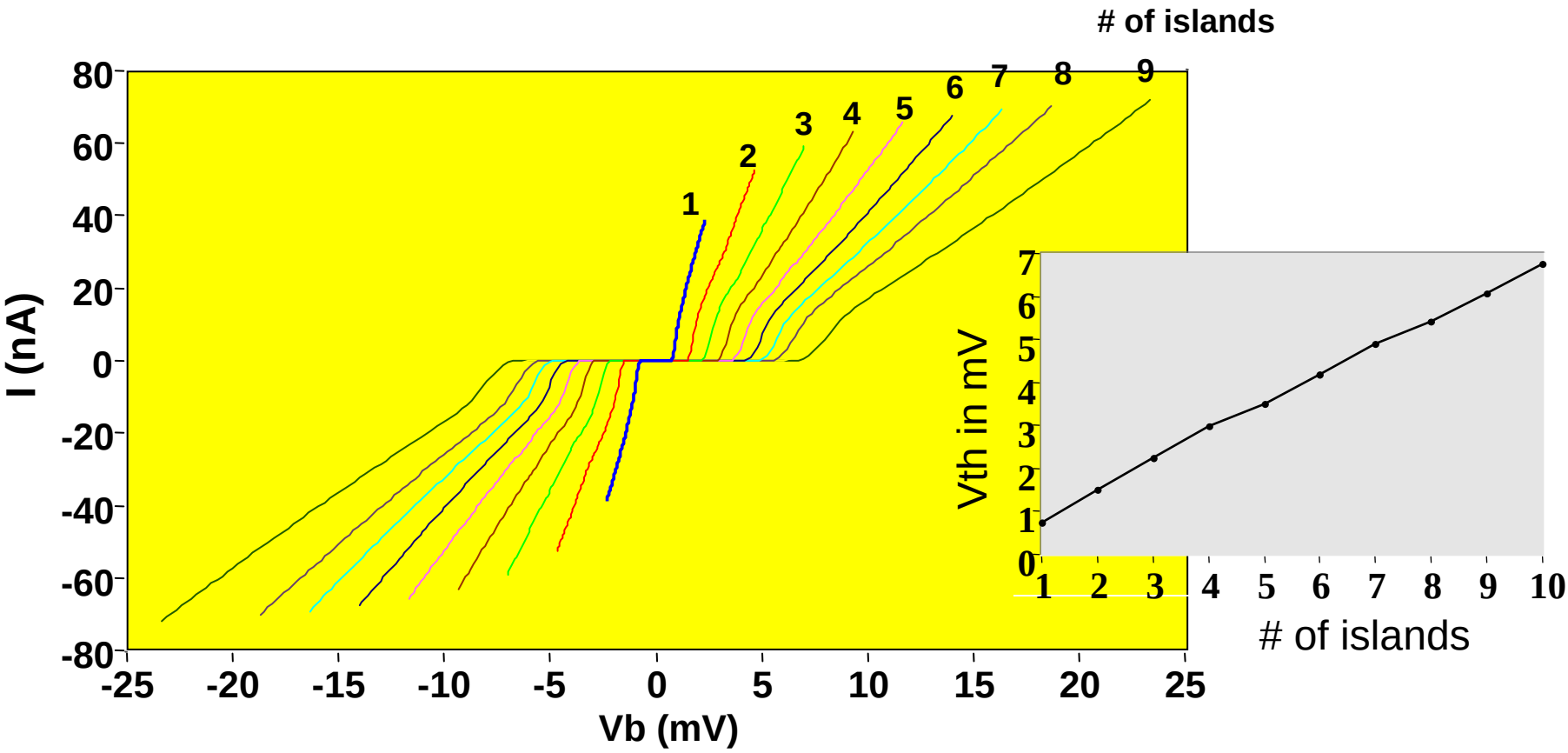

e/C=0.8mV

Vth in mV

0.747	1.495	2.243	2.991	3.497	4.197	4.890	5.403	6.078	6.753

A high strain two-stack two-color quantum well infrared photodetector

M. Z. Tidrow
Army Research Laboratory, AMSRL-SE-EI, Fort Monmouth, New Jersey 07703-5601

J. C. Chiang and Sheng S. Li
Department of Electrical and Computer Engineering, University of Florida, Gainesville, Florida 32611

K. Bacher
Quantum Epitaxial Designs, Inc., Bethlehem, Pennsylvania 18015

APL, 70, 859 (97)

FIG. 1. The schematic energy-band diagram of the two-stack, two-color InGaAs/AlGaAs MWIR and AlGaAs/GaAs LWIR QWIP.

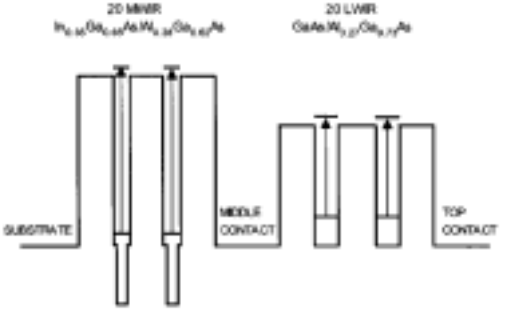

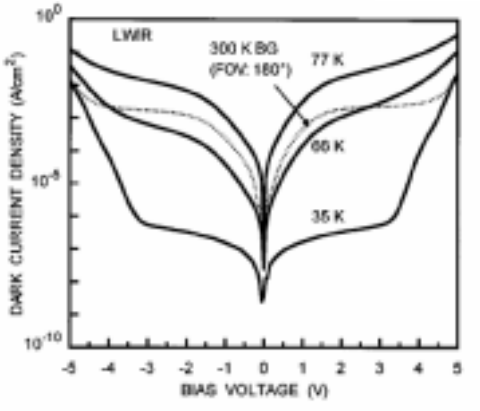

FIG. 3. The dark $J-V$ curves for the LWIR stack measured at 35, 66, and 77 K, along with the 300 K window current measured at 30 K with a field of view (FOV) 180°.

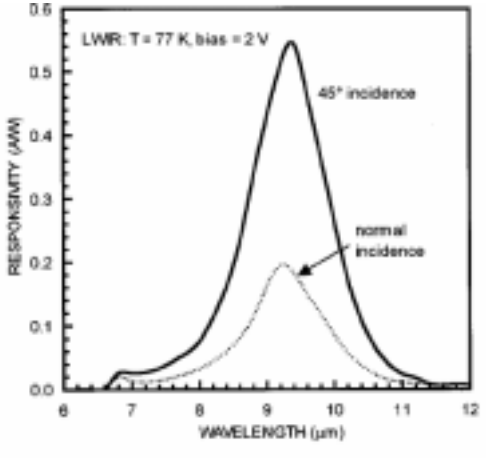

FIG. 7. The spectral responsivity for the LWIR stack measured at 2 V at 45° incidence (solid line) and normal incidence without grating (dashed line).

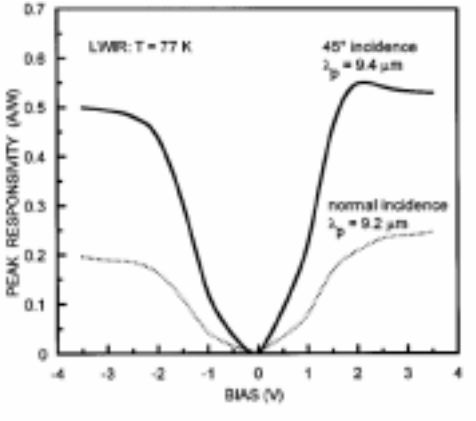

FIG. 6. The peak responsivity at $\lambda_p = 9.4$ μm vs bias voltage for the LWIR stack measured at 77 K at 45° incidence (solid line) and normal incidence without grating (dashed line).

Laser: light amplification by stimulated emission of light

Monochromatic, coherence

Requires:

1. **Atoms with discrete energy levels for laser emission transition**
2. **Population inversion**

Helium-Neon
Neodymium -YAG

Quantum dot laser : Quantum dots = atoms

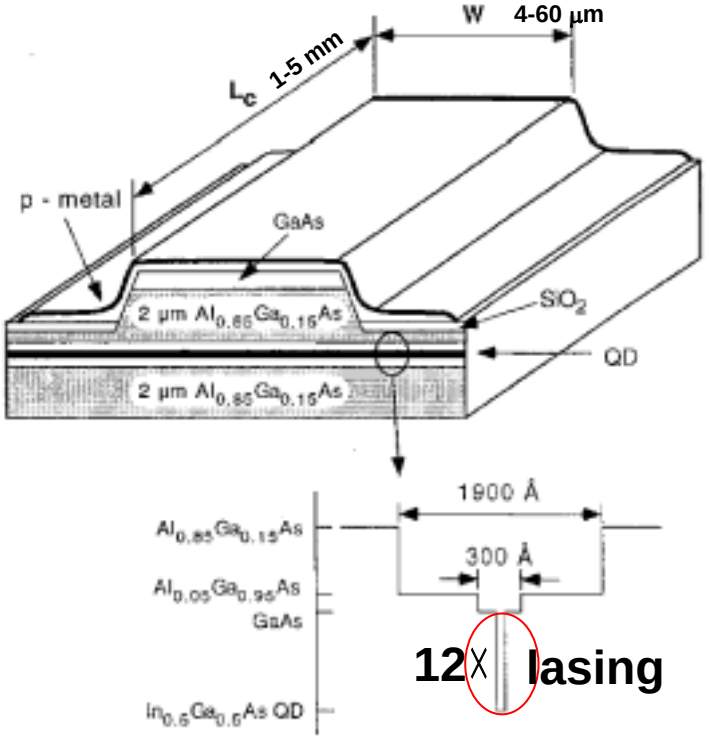

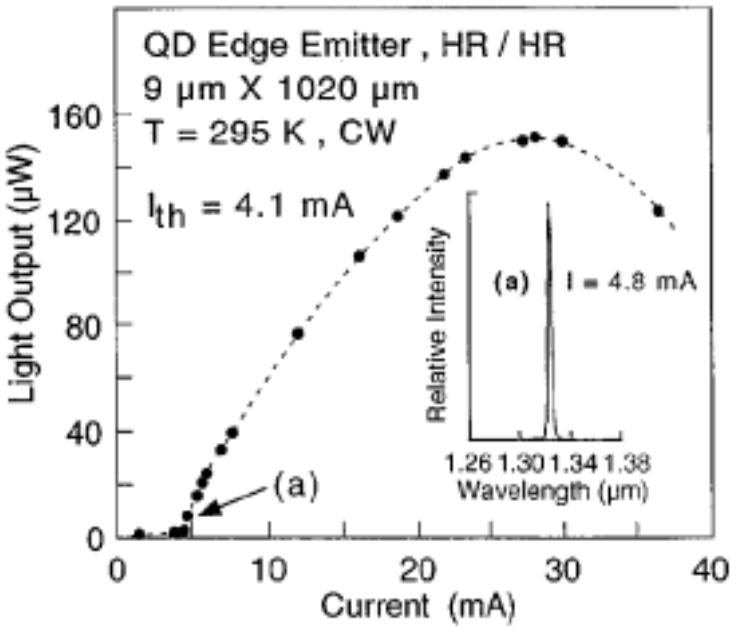

12 lasing

Superconductivity

Table 9.6. Transition temperatures T_c, coherence lengths ξ, and penetration depths λ of some typical superconductors

Material	Type	T_c (K)	ξ (nm)	λ (nm)
Cd	I	0.56	760	110
In	I	3.4	360	40
Pb	I	7.2	82	39
Pb–In alloy	II	7.0	30	150
Nb–N alloy	II	16	5	200
$PbMo_6S_8$	II	15	2	200
V_3Si	II	16	3	60
Nb_3Ge	II	23	3	90
K_3C_{60}	II	19	2.6	240

type I
type II

Source: Data are from C. P. Poole Jr, H. A. Farach, and R. J. Creswick *Superconductivity*, Academic Press, San Diego, 1995, p. 271.

A vortex core

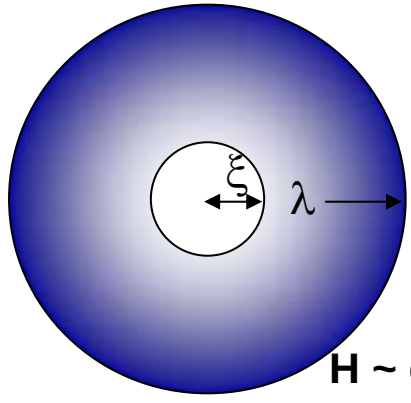

H ~ exp(r/λ)

enclose one flux quantum

$$\Phi_0 = \frac{h}{2e} = 2.0678 \times 10^{-15} Tm^2$$

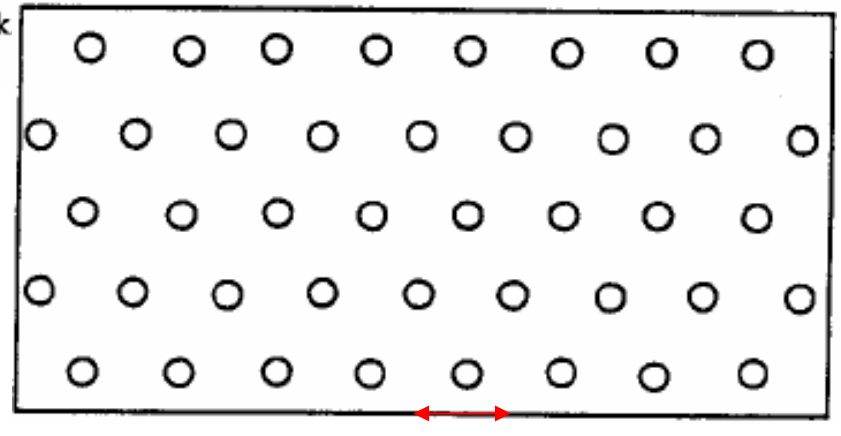

= λ at H_c1, ξ at H_c2

- Josephson effect

$$j = j_c \sin(\Delta\phi)$$

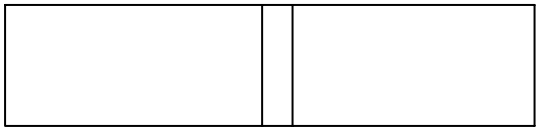

PHYSICAL REVIEW B VOLUME 39, NUMBER 16 P. 12260 1 JUNE 1989

Superconducting energy gap in Coulomb staircase tunneling structures

K. A. McGreer, J-C. Wan, N. Anand, and A. M. Goldman
School of Physics and Astronomy, University of Minnesota, Minneapolis, Minnesota 55455
(Received 21 November 1988)

J1=tip to Pb particle

J2=Pb particle to other Pb particles

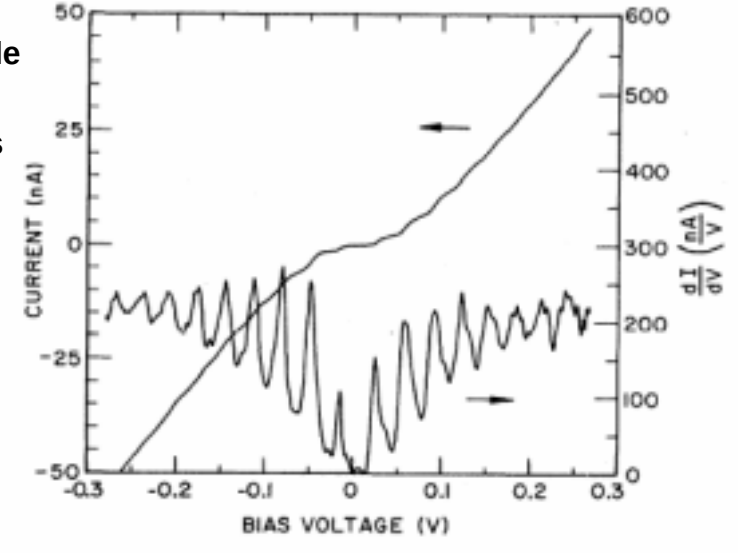

FIG. 1. Plots of I vs V and dI/dV exhibiting a clear Coulomb staircase. These were obtained from a tunneling structure formed between a granular Pb film and a STM tip.

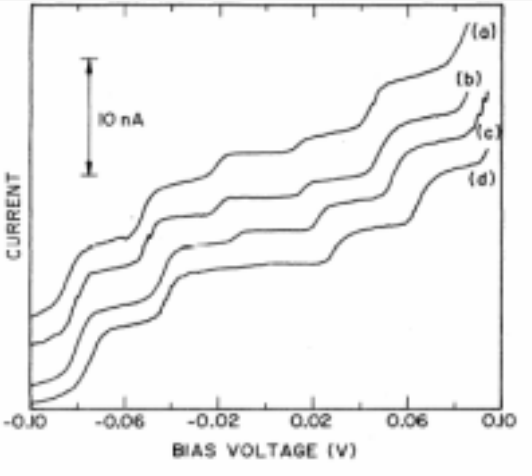

FIG. 3. Traces (a)–(d) show four different Coulomb staircase I-V characteristics with the STM tip in the same position. The traces are displaced vertically for clarity. Although the step widths are approximately the same for each trace, the steps occur at different bias voltages, that is, they have different values of Q_0. [See Eq. (2).] In (d) it is probable that a step edge occurs close to zero bias and is not resolved in this trace because the step height is too small.

Δ for Pb = 1.25±0.1meV

$$V_{\text{step}} = Q_0/C_1 + ne/C_1 + 4\Delta\,\text{sgn}(Q_0/C_1 + ne/C_1)$$